Journal of Magnetism and Magnetic Materials 386 (2015) 1–7

Contents lists available at ScienceDirect

Journal of Magnetism and Magnetic Materials

journal homepage: www.elsevier.com/locate/jmmm

Magnetic properties of a spin-1 triangular Ising system

Mehmet Ertaş [a], Yusuf Kocakaplan [b], Ersin Kantar [a,*]

[a] Department of Physics, Erciyes University, 38039 Kayseri, Turkey
[b] Graduate School of Natural and Applied Sciences, Erciyes University, 38039 Kayseri, Turkey

ARTICLE INFO

Article history:
Received 30 October 2014
Received in revised form
24 December 2014
Accepted 14 March 2015
Available online 17 March 2015

Keywords:
Triangular lattice
Site dilution
Phase diagram
Hysteresis behavior
Susceptibility
Effective-field theory

ABSTRACT

We studied some magnetic behaviors of the Blume-Capel (BC) model in a site diluted triangular lattice by means of the effective-field theory (EFT) with correlations. The effects of the exchange interaction (J), crystal field (D), concentration (p) and temperature (T) on the magnetic properties of the spin-1 BC model in a triangular lattice, such as magnetization, susceptibility, phase diagram and hysteresis behaviors, are investigated in detail. The phase diagrams of the system are presented in two different planes. The tricritical point as well as the tetracritical and critical end special points are found to depend on the physical parameters of the system. Moreover, when the hysteresis behaviors of the system are examined, single and double hysteresis loops are observed for various values of the physical parameters. We show that the hysteresis loops have different coercive field points in which the susceptibility makes a peak at these points.

1. Introduction

In the triangular lattice, local geometric constraints prevent simultaneous minimization of all the pairwise interactions. Thus, the Ising model with the nearest-neighbor antiferromagnetic interactions on a triangular lattice is fully frustrated. Recently, the triangular lattice structure has increasingly attracted much interest due to the fact that it has been used the prototypical modeling of some real magnetic materials, such as $CsCoX_3$ (X=Cl or Br) and $Ca_3Co_2O_6$ spin-chain compounds, and for low-temperature and high-degenerate cases showing different behaviors [1–3]. Žukovič [4] employed a thermodynamic integration method to establish the values of the residual entropy for the geometrically frustrated spin-S triangular Ising antiferromagnet, with the spin values $S=1/2, 1, 3/2, 2$ and $5/2$. He obtained an analytical formula for the lower bound in a general spin-S model and conjecture that it should reasonably approximate the true residual entropy for sufficiently large S. The first-order [5] and second-order [6] phase transitions features of the triangular Ising model with the nearest- and next-nearest-neighbor antiferromagnetic interactions have been studied by using a Wang–Landau entropic sampling scheme. By utilizing the EFT with correlations, Žukovič et al. [7] investigated the magnetization processes and phase transitions in a geometrically frustrated triangular lattice Ising antiferromagnet in the presence of a random site dilution and an external magnetic field. They found that the interplay between the applied field and the frustration-relieving dilution results in peculiar phase diagrams in the temperature-field-dilution parameter space. Melchert and Hartmann [8] presented an algorithm for the computation of ground state spin configurations for the $2d$ random bond Ising model on a triangular lattice. They also investigated the critical behavior of the corresponding $T=0$ ferromagnet to spin-glass transition, signaled by a breakdown of the magnetization, using finite-size scaling analyses of the magnetization. The triangular Blume-Capel (BC) model has been studied by using Monte-Carlo simulations (MCs) and discussed that the effects of bond randomness on the universality aspects of a two dimensional BC model embedded in a triangular lattice have been discussed [9]. Žukovič et al. [10] examined the effects of selective dilution on the phase diagrams and ground-state magnetizations of the spin-1/2 Ising antiferromagnetic model by using EFT. They found that the obtained results showed a fairly good agreement with previous studies using different methods. Low-temperature magnetization processes in a stacked triangular Ising antiferromagnet have been studied [11] in detail by utilizing MCs, and multiple steps and hysteresis corresponding to the formation of different metastable states were observed in increasing and decreasing magnetic fields. Borovský et al. [12] studied the critical and tricritical behaviors of a selectively diluted triangular Ising antiferromagnet by using both EFT and MCs. In particular, they focused on the effects of the frustration-relieving selective dilution on the phase diagram and found that it can lead to rather intricate phase diagrams in the dilution-field parameters space. Žukovič and Bobák [13]

* Corresponding author. Fax: +90 352 4374901.
E-mail address: ersinkantar@erciyes.edu.tr (E. Kantar).

http://dx.doi.org/10.1016/j.jmmm.2015.03.058
0304-8853/

investigated the critical behavior of the BC antiferromagnet on a triangular lattice by MCs and found two kinds of phases within the single-ion anisotropy strength $-1.47 < \Delta < 0$. They found that there is only one phase transition from the long-range ordering to the paramagnetic region and the transition is of first order for $-1.57 < \Delta < -1.47$. Žukovič and Bobák [14] also studied the critical behaviors of a geometrically frustrated spin-1 Ising antiferromagnet on a triangular lattice in the presence of a single-ion anisotropy by employing MCs. They showed that the presence of the single-ion anisotropy can lead to a partial long-range order in the low-temperature region even below the critical value, namely for the spin-1, within a certain range of the anisotropy strength. They also studied densities of various local spin patterns in the respective phases. Moreover, by using the position-space renormalization group (PSRG) [15] and transfer matrix [16] methods, a frustrated antiferromagnetic spin-1 BC model on a triangular lattice was examined and found to display a finite-temperature antiferromagnetic (AF) LRO of the type (1, −1, 0) within a certain range of the single-ion anisotropy strength, accompanied by a multicritical behavior.

In spite of these studies, to the best of our knowledge, the magnetization, susceptibility, phase diagram and hysteresis behaviors of the BC model in a site diluted triangular lattice by means of the EFT with correlations have not been investigated, in detail. Therefore, in this paper, we have studied the influences of the exchange interaction (J), crystal field (D), concentration (p) and temperature (T) on the magnetic properties of the spin-1 BC model in a triangular lattice. We should also mention that the ferromagnets have wide applications, such as a "soft" ferromagnet in a transformer core and a "hard" permanent magnets in hard disk, and in magnetic tape and motors depending on the extent of the hysteresis loop, see [16] and [17]. The further development of materials with hysteresis needs a deep understanding of their microscopic interactions and how these interactions influence their hysteresis phenomena [18].

The paper is arranged as follows. In Section 2, we give the model and present the formalism of the model in the EFT. The detailed numerical results and discussions are presented in Section 3. Finally Section 4 is devoted to a summary and a brief conclusion.

2. Model and formalism

Under the Blume-Capel model the Hamiltonian of spin-1 Ising model can be written as

$$H = -J\sum_{\langle ij\rangle} S_i S_j - D\sum_i S_i^2 - h\sum_i S_i \tag{1a}$$

where S_i is the Ising spin and it takes $S_i = \pm 1,\ 0$ values, D is the crystal field or single-ion anisotropy, h is the external magnetic field, J is the exchange interaction parameter and $\langle i,\ j\rangle$ denotes the summation over all the nearest-neighbor pairs. Moreover, the Hamiltonian of the selectively diluted triangular lattice, which includes the nearest-neighbor interactions and the crystal field, is given as follows:

$$H = -J\sum_{\langle ij\rangle} \xi_i \xi_j S_i S_j - D\sum_i \xi_i S_i^2 - h\sum_i \xi_i S_i \tag{1b}$$

The parameter ξ_i is a site occupancy number that is 1 or zero, depending on whether the site is occupied or not. Since only the surface is diluted in the present system, ξ_i are quenched, uncorrelated random variables chosen to be equal to 1 with probability p, when the site i is occupied by a magnetic atom and 0, with probability $1-p$ otherwise. Then the probability distribution is given by $P(\xi_i)=p\delta(\xi_i - 1) + (1-p)\delta(\xi_i)$ and p represents the mean concentration of magnetic sites. These facts are seen explicitly using the EFT on the different systems such as in a triangular lattice [10,19], an ultrathin Ising film [20], and on a honeycomb lattice [21].

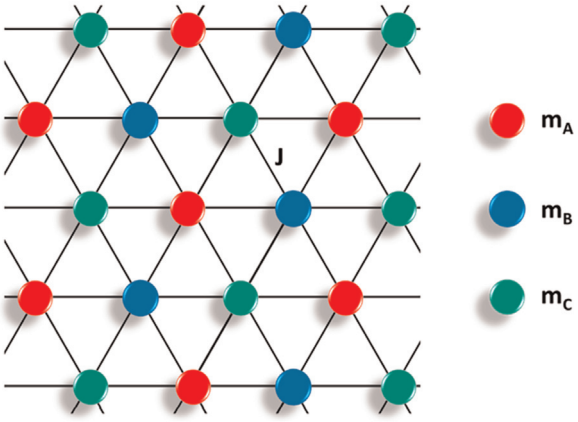

Fig. 1. Schematic representation of triangular Ising system. The red, blue, and green spheres indicate magnetic atoms at m_A, m_B, m_C, respectively. (For interpretation of the references to color in this figure legend, the reader is referred to the web version of this article.)

Within the framework of the EFT with correlations, one can easily find the sublattice magnetizations, and the quadrupolar moment terms as coupled equations for the diluted triangular lattice as follows:

$$m_A = \left[p\left(1 + m_B\ \sinh(J\nabla) + m_B^2(\cosh(J\nabla)-1)\right) + 1 - p\right]^3 \left[p\left(1 + m_C\ \sinh(J\nabla) + m_C^2(\cosh(J\nabla)-1)\right) + 1 - p\right]^3 F(x)\big|_{x=0} \tag{2a}$$

$$m_B = \left[p\left(1 + m_A\ \sinh(J\nabla) + m_A^2(\cosh(J\nabla)-1)\right) + 1 - p\right]^3 \left[p\left(1 + m_C\ \sinh(J\nabla) + m_C^2(\cosh(J\nabla)-1)\right) + 1 - p\right]^3 F(x)\big|_{x=0}, \tag{2b}$$

$$m_C = \left[p\left(1 + m_A\ \sinh(J\nabla) + m_A^2(\cosh(J\nabla)-1)\right) + 1 - p\right]^3 \left[p\left(1 + m_B\ \sinh(J\nabla) + m_B^2(\cosh(J\nabla)-1)\right) + 1 - p\right]^3 F(x)\big|_{x=0}, \tag{2c}$$

$$q_A = \left[p\left(1 + m_B\ \sinh(J\nabla) + m_B^2(\cosh(J\nabla)-1)\right) + 1 - p\right]^3 \left[p(1 + m_C\ \sinh(J\nabla) + m_C^2 + 1 - p\right]^3 G(x)\big|_{x=0}, \tag{3a}$$

$$q_B = \left[p\left(1 + m_A\ \sinh(J\nabla) + m_A^2(\cosh(J\nabla)-1)\right) + 1 - p\right]^3 \left[p\left(1 + m_C\ \sinh(J\nabla) + m_C^2(\cosh(J\nabla)-1)\right) + 1 - p\right]^3 G(x)\big|_{x=0}, \tag{3b}$$

$$q_C = \left[p\left(1 + m_A\ \sinh(J\nabla) + m_A^2(\cosh(J\nabla)-1)\right) + 1 - p\right]^3 \left[p\left(1 + m_B\ \sinh(J\nabla) + m_B^2(\cosh(J\nabla)-1)\right) + 1 - p\right]^3 G(x)\big|_{x=0}, \tag{3c}$$

where $\nabla = \partial/\partial x$ is the differential operator. The functions $F(x)$ and $G(x)$ are defined as

$$F(x) = \frac{2\sinh[\beta(x+h)]}{\exp(-\beta D) + 2\cosh[\beta(x+h)]} \tag{4a}$$

$$G(x) = \frac{2\cosh[\beta(x+h)]}{\exp(-\beta D) + 2\cosh[\beta(x+h)]} \tag{4b}$$

Here, $\beta = 1/k_B T$, T is the absolute temperature and k_B is the

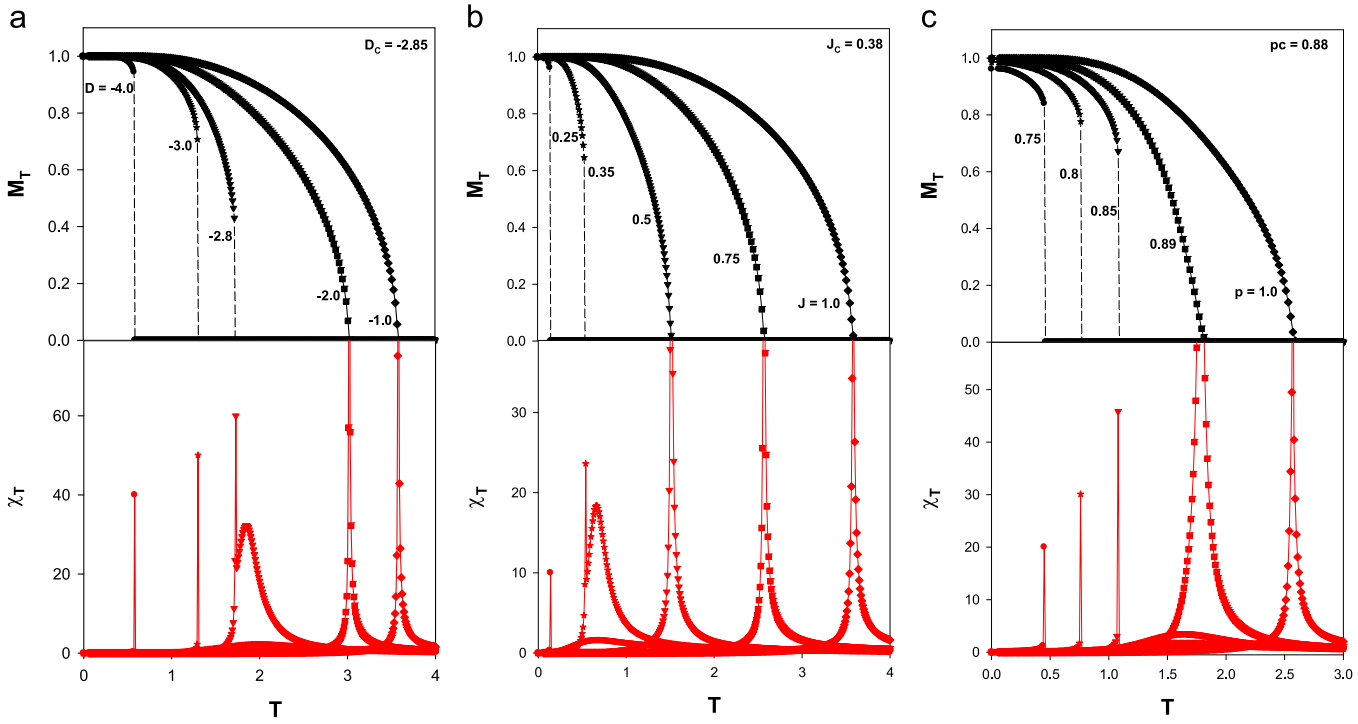

Fig. 2. Thermal variations of the magnetizations and susceptibilities with various values of p, J and D. (a) $p=1.0$, $J=1.0$ and $D=-4.0$, -3.0, -2.8, -2.0, -1.0. (b) $p=1.0$, $D=1.0$ and $J=$ 0.25, 0.35, 0.5, 0.75, 1.0. (c) $J=1.0$, $D=1.0$ and $p=0.75$, 0.8, 0.85, 0.89, 1.0.

Boltzmann constant. By using the definitions of the order parameters in Eqs. (2a)–(2c), the total m_T magnetizations of each site can be defined as $m_T = 1/3(m_A + m_B + m_C)$.

In order to obtain the susceptibilities of the system, we differentiated magnetizations with respect to h as in the following equation:

$$\chi_\alpha = \lim_{\to 0}\left(\frac{\partial m_\alpha}{\partial h}\right) \tag{5}$$

where, $\alpha=A$, B and C. By using Eqs. (2) and (5), we can easily obtain the χ_A, χ_B and χ_S susceptibilities as follows:

$$\chi_A = a_1\chi_B + a_2\chi_C + a_3\frac{\partial F(x)}{\partial h} \tag{6a}$$

$$\chi_B = b_1\chi_A + b_2\chi_C + b_3\frac{\partial F(x)}{\partial h} \tag{6b}$$

$$\chi_C = c_1\chi_A + c_2\chi_B + c_3\frac{\partial F(x)}{\partial h} \tag{6c}$$

Here, the a_i, b_i and c_i ($i=1$, 2 and 3) coefficients have complicated and long expressions, hence they will not give. The total susceptibility of each site can be obtained via $\chi_T = 1/3(\chi_A + \chi_B + \chi_C)$.

On the other hand, in order to obtain the second-order phase transition temperatures as well as the phase diagram, we must expand the right-hand sides of (2a)–(2c) coupled equations. They are obtained as follows:

$$Am = \begin{pmatrix} 0 & k_1 & k_2 \\ m_1 & 0 & m_2 \\ n_1 & n_2 & 0 \end{pmatrix}\begin{pmatrix} m_A \\ m_B \\ m_C \end{pmatrix} = 0 \tag{7}$$

Here, the coefficients k_i, m_i and n_i in each matrix have complicated forms, so that they will not give. These coefficients can be easily obtained from the coupled equations via the differential operator technique. The second-order phase transition temperatures of each system can be determined from det $(A)=0$. Moreover, to obtain the first-order phase transition temperatures, we have to solve Eqs. (2a)–(2c) numerically. In this way, we can obtain the tricritical point (TCP) by using the existence of the first- and second-order phase transition points.

By solving these equations, we can obtain the numerical results of the spin-1 diluted triangular lattice. We will give these results in the next section.

3. Numerical results and discussions

In this section our attention is focused on the study of the magnetic properties, the phase diagrams and hysteresis behavior of a spin-1 Triangular Ising system (TIS) with a crystal field interaction.

3.1. Magnetic properties of magnetizations and susceptibilities

The thermal behavior of Fig. 1 the total magnetizations (M_T) and susceptibilities (χ_T) of the spin-1 TIS are plotted in Fig. 2. In Fig. 2(a)–(c), we investigated the behavior of the first- and second-order phase transition points, as well as the tricritical point, for different values of the crystal field, the bilinear interaction parameter and the concentration. Thus, this study led us to characterize the transitions as well as to obtain the transition points. Fig. 2(a) is obtained for fixed values $J=1.0$ and $p=1.0$, and the selected values of D, i.e., -4.0, -3.0, -2.8, -2.0 and -1.0. In this figure for $D=-4.0$, -3.0 and -2.8 values, the total magnetizations go to zero discontinuously as the temperature increases; hence, a first-order phase transition occurs. On the other hand, for $D=-2.0$ and -1.0 values the total magnetizations decrease continuously with the increase in temperature values below the critical temperature and they become zero; hence, a second-order phase transition occurs. Moreover, in Fig. 2(b) and (c) for low

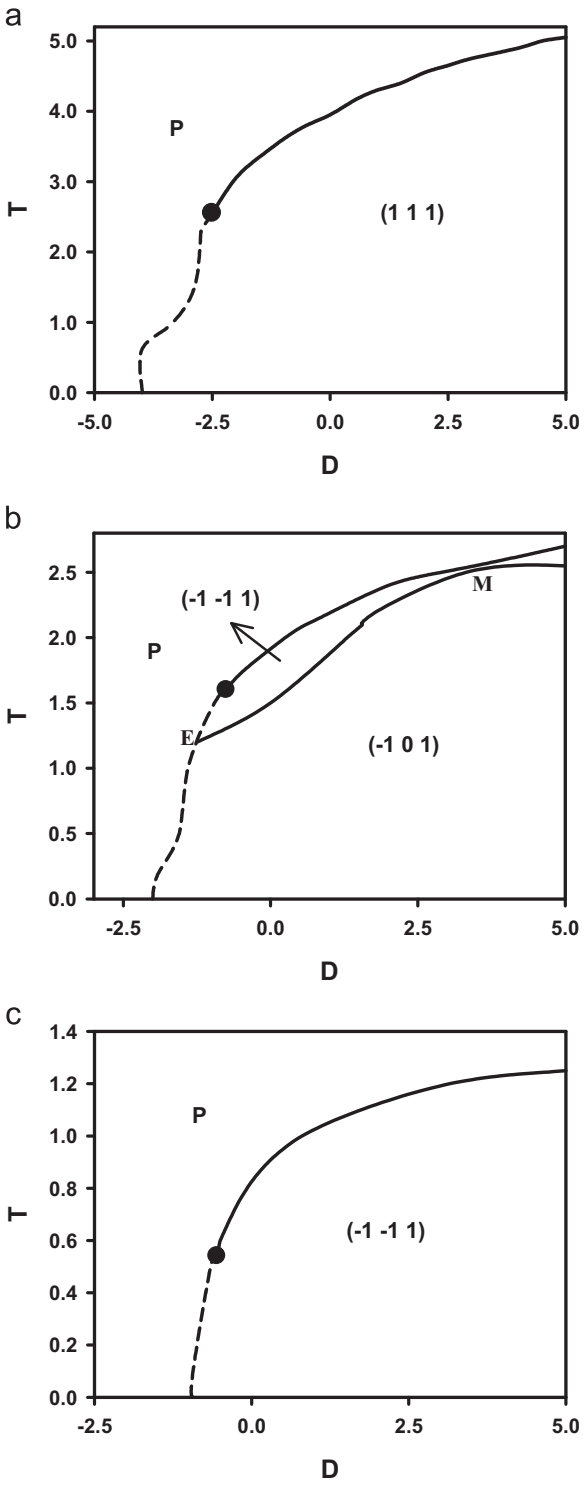

Fig. 3. The phase diagrams in (T–D) plane of the triangular Ising system. Dashed and solid lines represent the first- and second-order phase transitions, respectively. (a) $J=1.0$ and $p=1.0$. (b) $J=-1.0$ and $p=1.0$. (c) $J=-1.0$ and $p=0.5$.

values of J and p, namely $J=0.25$ and 0.35 values and $p=0.75$, 0.80, and 0.85 values, the system illustrates first-order phase transitions; the system exhibits a second-order phase transition for high values of J and p. In the system, the critical values are obtained as $D_C=-2.85$, $J_C=0.38$, and $p_C=0.88$, for the crystal field, bilinear interaction parameter and the concentration. The susceptibilities diverge as the temperature approaches the critical temperature in Fig. 2. When D, J, and p take higher values, the susceptibility

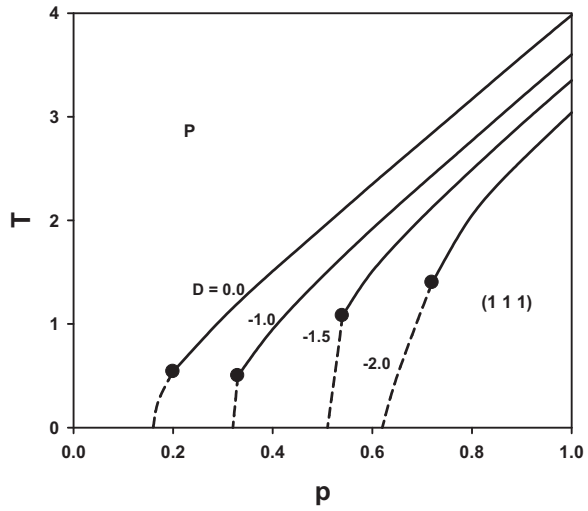

Fig. 4. The phase diagrams in (T–p) plane of the triangular Ising system. Dashed and solid lines represent the first- and second-order phase transitions, respectively. For $J=1.0$ and $D=0.0$, -1.0, -1.5, -2.0.

divergence at the critical temperature shifts to higher temperatures. However, when D, J, and p take lower values, they become finite and display a jump singularity behavior at the first-order phase transition.

3.2. Phase diagrams

In this subsection, we will show some typical results for the TIS with a crystal field. We obtained the phase diagrams in two different planes, namely (D, T) and (p, T) for TIS.

3.2.1. Phase diagrams in (D, T) plane

At first, we present the phase diagrams of the model in the (D, T) plane, as illustrated in Fig. 3. In these phase diagrams, the solid and dashed lines represent the second- and first-order phase transition lines, respectively, and the tricritical points are denoted by filled circles. It is clear that the second- and first-order phase transition lines separate the ordered phases, namely (1, 1, 1), (-1, -1, 1) and (-1, 0, 1) from the paramagnetic (P) phase. From these phase diagrams the following phenomena were observed. (1) Each of the phase diagrams exhibits only one tricritical point where the second-order phase transition turns into a first-order one. (2) In Fig. 3(a), the reentrant behavior exists in the TIS, i.e., the system has a disordered (paramagnetic) phase at very low temperatures and as the temperature increases the system has an antiferromagnetic (1, 1, 1) phase at a critical temperature T_{c1} and finally a paramagnetic phase at a higher critical temperature T_{c2}. (3) In Fig. 3(b), are observed the special critical points, namely critical end point (E) and tetracritical point (M) in the system.

3.2.2. Phase diagrams in (p, T) plane

In Fig. 4, the phase diagram of spin-1 TIS is obtained in order to examine the influence of the interfacial coupling, namely J. Fig. 4 shows the variations of T as a function of p, when the parameter J is fixed at $J=1.0$ and the value of D is changed ($D=0.0$, -1.0, -1.5 and -2.0). In Fig. 4, the phase transition region is divided into two phases, namely P and (1, 1, 1). From Fig. 4, we can see that the phase transitions are second-order and first-order phase transitions for high and low values of temperature, respectively. When the crystal field takes higher values, the tricritical points are obtained at lower temperature.

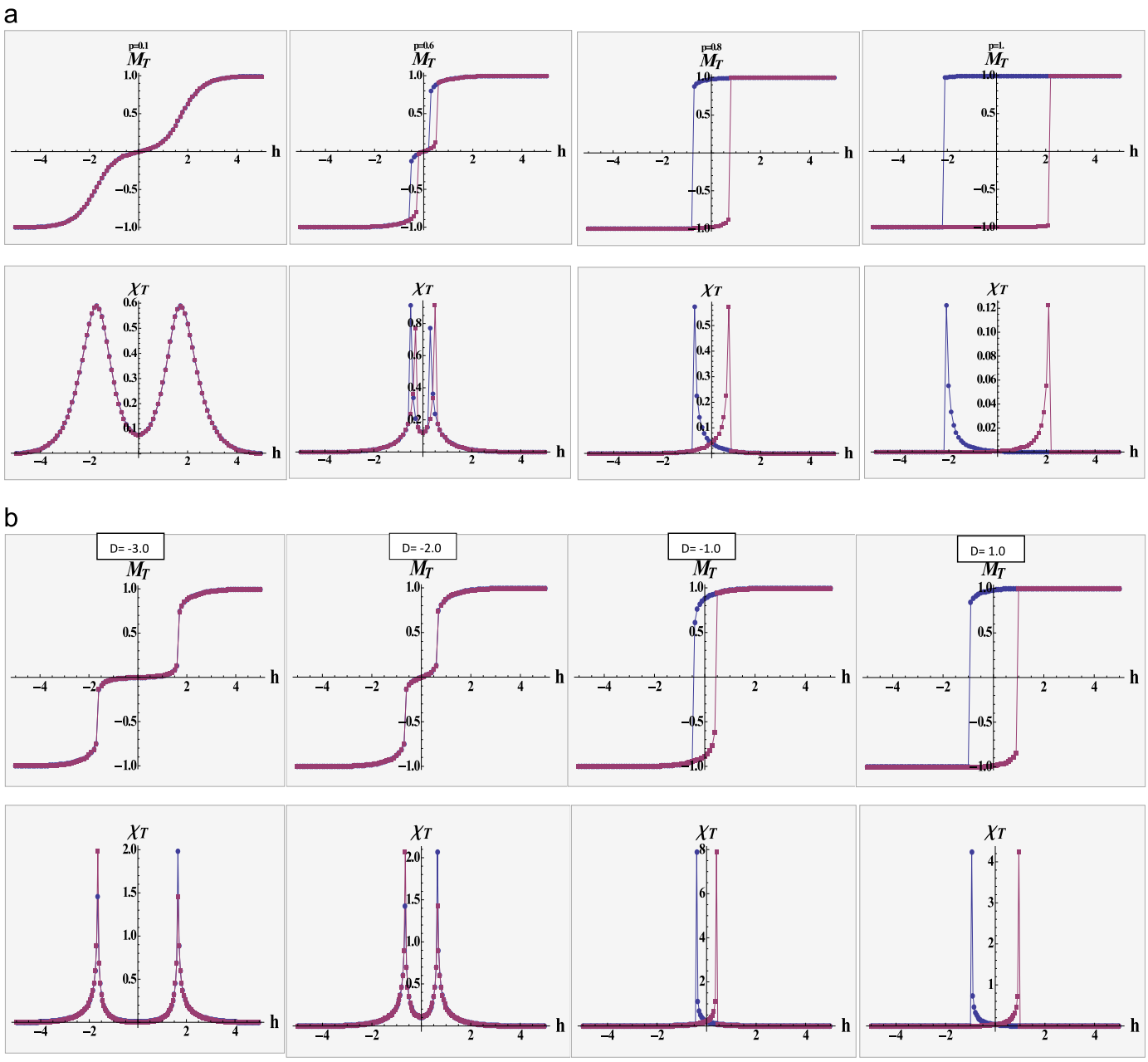

Fig. 5. Hysteresis behaviors of triangular Ising system. (a) $D=-2.0$, $J=0.5$, $T=1.0$ and $p=0.3$, 0.6, 0.8, 1.0. (b) $J=1.0$, $T=0.5$, $p=0.5$ and $D=-3.0$, -2.0, -1.0, 1.0. (c) $D=0.0$, $T=0.5$, $p=0.5$ and $J=0.1$, 0.5, 0.7, 1.0. (d) $D=0.0$, $J=0.5$, $p=0.5$ and $T=0.1$, 0.5, 0.7, 1.1.

3.3. *Hysteresis behaviors*

Our aim in this subsection is to examine the effects of the crystal field, concentration, bilinear interaction, and temperatures on the hysteresis behaviors of a spin-1 TIS. Fig. 5(a) is obtained for four selected typical concentration values, namely $p=0.3$, 0.6, 0.8, 1.0 in the case of $D=-2.0$, $T=0.5$ and $J=1.0$ fixed values to investigate the temperature dependence of the hysteresis and susceptibility behaviors of the spin-1 TIS. With the increase of the crystal field parameter, the double hysteresis loop becomes a single hysteresis loop and the single hysteresis loop becomes wider. In Fig. 5(b), similar hysteresis loop behaviors as those in Fig. 5(a) are observed for the increasing values of D. The total susceptibility peaks confirm the above calculations. In Fig. 5(c), the hysteresis loops area increases as the bilinear parameter increases. This fact is also understood from the susceptibility peak having two values in both directions of the external magnetic field. In Fig. 5(d), the hysteresis loops area decreases as the temperature increases. This fact is also understood from the susceptibility peak turn to reaches a single value in both directions of the external magnetic field. The physical explanation for this fact is that while at low temperatures the system becomes hard magnet, with the increase of the temperature the hard magnet turns to soft magnet. These results are consistent with some experimental results [22–25].

4. Summary and conclusion

In this study, we studied some magnetic behaviors of the Blume-Capel (BC) model in a site diluted triangular lattice by means of the effective-field theory (EFT) with correlations. We investigated the magnetic properties of the spin-1 BC model in a triangular lattice in detail. We also obtained the phase diagrams of

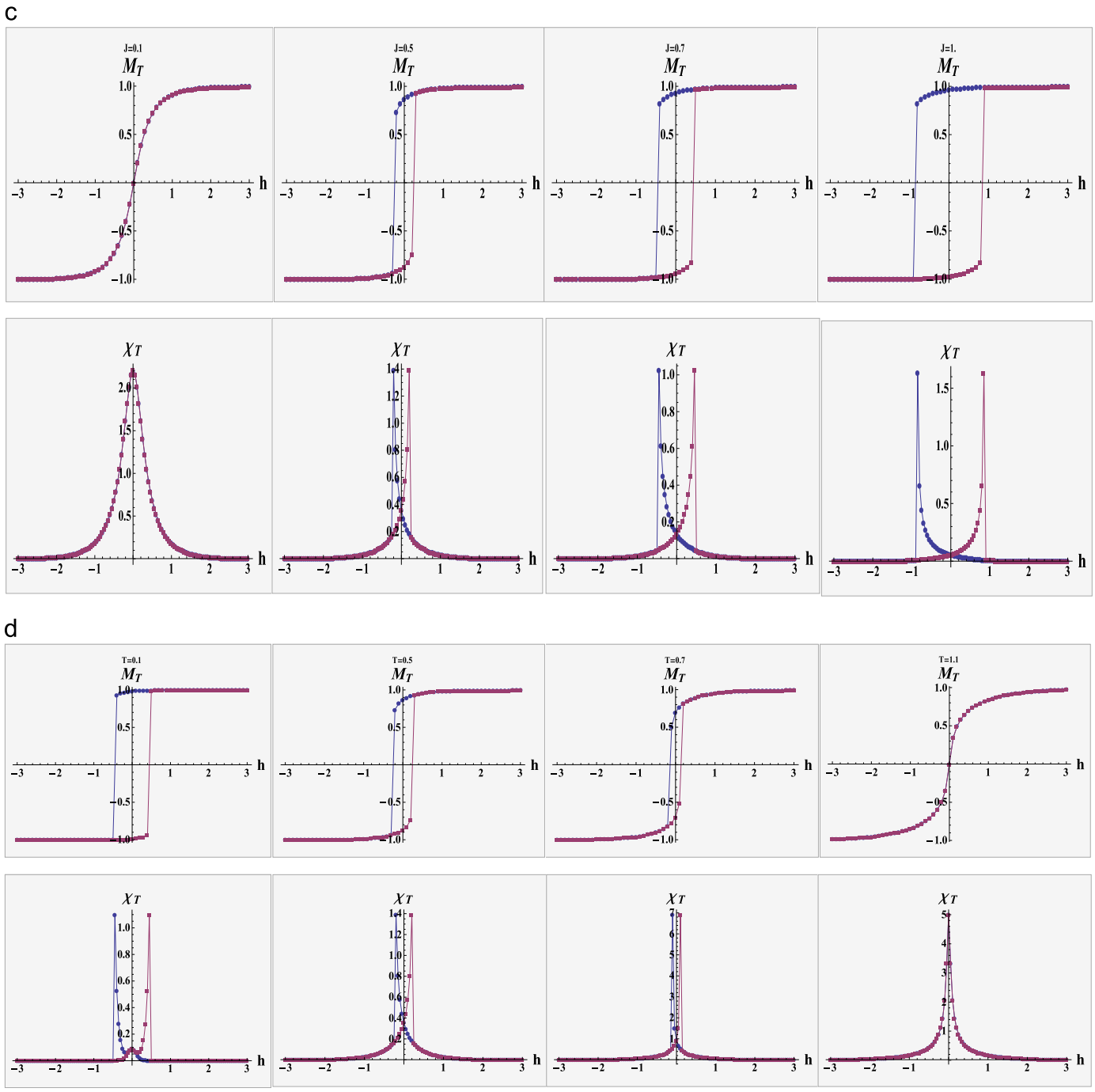

Fig. 5. (*continued*)

the system in two different planes. The tricritical point as well as the tetracritical and critical end special points are found to depend on the physical parameters of the system. Moreover, when the hysteresis behaviors of the system are examined, single and double hysteresis loops are observed for various values of the physical parameters. We show that the hysteresis loops have different coercive field points and that the susceptibility makes a peak at these points.

Finally, the comparison of our results with Ref. [9], same system, but different method, namely MCs, is as follows: (1) the system within the EFT shows the tricritical point as well as the tetracritical and critical end special points, but the system within the MCs displays only a tricritical point. (2) Three different ordered phases, namely (1 1 1), (−1, −1, 1), (−1, 0, 1), is observed when using the EFT, but defines only one ordered phase when using the MCs. (3) The system within the EFT has three fundamental phase diagrams in the (D, T), but the system within the MCs has one fundamental phase diagram.

Acknowledgements

This work was supported by the Scientific and Technological Research Council of Turkey (TUBITAK) (Grant no: 114F008) and

Erciyes University Research Funds (Grant no: FDA-2014-5188).

References

[1] V. Hardy, M.R. Lees, O.A. Petrenko, D.M. Paul, D. Flahaut, S. Hébert, A. Maignan, Phys. Rev. B 70 (2004) 064424.
[2] Y. Kudasov, Phys. Rev. Lett. 96 (2006) 027212.
[3] R. Soto, G. Martínez, M.N. Baibich, J.M. Florez, P. Vargas, Phys. Rev. B 79 (2009) 184422.
[4] M. Žukovič, Eur. Phys. J. B 86 (2013) 283.
[5] A. Malakis, N.G. Fytas, P. Kalozoumis, Physica A 383 (2007) 351.
[6] N.G. Fytas, A. Malakis, Physica A 388 (2009) 4950.
[7] M. Žukovič, M. Borovský, A. Bobák, Phys. Lett. A 374 (2010) 4260.
[8] O. Melchert, A.K. Hartmann, Comp. Phys. Commun. 182 (2011) 1828.
[9] P.E. Theodorakis, N.G. Fytas, Phys. Rev. E 86 (2012) 011140.
[10] M. Žukovič, M. Borovský, A. Bobák, J. Magn. Magn. Mater. 324 (2012) 2687.
[11] M. Žukovič, L. Mizisin, A. Bobák, Phys. Lett. A 376 (2012) 1731.
[12] M. Borovský, M. Žukovič, A. Bobák, Physica A 392 (2013) 157.
[13] M. Žukovič, A. Bobák, Phys. Rev. E 87 (2013) 032121.
[14] M. Žukovič, A. Bobák, J. Kor., Phys. Soc. 62 (2013) 1495.
[15] G.D. Mahan, S.M. Girvin, Phys. Rev. B 17 (1978) 4411.
[16] J.B. Collins, P.A. Rikvold, E.T. Gawlinski, Phys. Rev. B 38 (1988) 6741.
[17] C. Leighton, Physics **3** (2010) 79.
[18] A.A. Bukharov, A.S. Ovchinnikov, N.V. Baranov, K. Inoue, J. Phys.: Condens. Matter 22 (2010) 436003.
[19] M. Borovský, M. Žukovič, A. Bobák, Acta Phys. Pol. A 126 (2014) 16.
[20] T. Kaneyoshi, Physica B 436 (2014) 208.
[21] Z.-L. Wang, Z.-Y. Li, J. Phys. Condens. Matter **2** (1990) 8615.
[22] B.Z. Mi, H.Y. Wang, Y.S. Zhou, J. Magn. Magn. Mater. 322 (2010) 952.
[23] H. Zeng, S. Sun, J. Li, Z.L. Wang, J.P. Liu, Appl. Phys. Lett. 85 (2004) 792.
[24] J.A. Garcia, E. Bertran, L. Elbaile, J.G. Cespedes, A. Svalov, Phys. Status Solidi C 7 (2010) 2679.
[25] O. Iglesias, A. Labarta, Phys. Rev. B 63 (2001) 184416.